SHEAR BAND DEVELOPMENT IN MODIFIED DEM: IMPORTANCE OF COUPLE STRESS

KAZUYOSHI IWASHITA AND MASANOBU ODA

Deptartament of Civil and Environmental Engineering
Saitama University
Urawa, Saitama 338, Japan

Abstract: Numerical simulation tests were carried out using the distinct element method (DEM) with great interest in how large couple stress is actually generated in a shear band. To do this, the conventional DEM was modified slightly, so that the effect of rolling resistance at contact points can be taken into account (called MDEM). It has been found that MDEM provides a powerful tool in simulating not only the generation of large voids inside a shear band but also the high gradient of particle rotation along the shear band boundaries, in a quite similar manner to those of natural granular soils; and that couple stress, although it is very small, is certainly developed in a consistent manner with the particle rotation gradient developed in a shear band.

1. Intoduction

In a plane strain test of a dense granular soil, homogeneous deformation first takes place. Around a peak stress, the deformation suddenly localizes into narrow zones (called the shear bands), and the stress drops sharply down to a residual stress state. Such a strain localization phenomenon is of great importance since soil engineering problems such as earth pressure, bearing capacity and slope stability are usually analyzed by assuming that the failure takes place along the shear band. In order to clarify the mechanical meaning of shear band, many research works have already been done for the past four decades in the field of soil mechanics (e.g., Newland & Allely, 1957; Rowe, 1962; Matsuoka, 1974; and Nemat-Nasser, 1980). Also, the strain localization problem is still a hot topic in the theoretical, as well as experimental, study of granular soil (e.g., Scarpelli & Wood, 1892; Mühlhaus & Vardoulakis, 1987; Vermeer, 1990; Tatsuoka, et al., 1990; Yoshida, et al., 1994; Finno, et at., 1996; and Desrues, et al., 1996).

It should be emphasized here that the basic mechanism leading to a shear band is not understood well, in spite of the extensive studies. In order to overcome the present difficulty, soil engineers are paying more attention to numerical simulation methods since the micro-process of shear band development can be directly observed in them (e.g., Cundall, 1971; Cundall & Strack, 1979; Bathurst & Rothenburg, 1990; Bardet & Proubet, 1991 and 1992; Iwashita, et al., 1995; Ke & Bray, 1995; and Thomas et al., 1996). To obtain this, however, a question must

be answered: does such a conventional numerical simulation method provide a sound basis for simulating the micro process of the shear band development, as well as the overall stress-strain behavior?

Oda (1997) and Oda and Kazama (1998) recently observed micro-structure of shear bands developed in several natural sands, by means of X-ray application and an optical method using a microscope and thin sections. Two observations are worth noting here: very large voids are generated in shear bands in parallel with strong strain localization, and as a result of this, the void ratio can exceed the corresponding maximum one determined by a standard method; and particles rotate extensively in the shear band so that a high particle rotation gradient is generated along the shear band boundaries. An important point is that nobody has succeeded in reproducing such huge voids and a high rotation gradient by any conventional numerical methods. In other words, there might be something to be done in order to improve such conventional methods. This is the motivation of starting the present study.

Each particle can move against neighboring particles through sliding and rolling at contact points. The sliding plays a dominant role in classical theories of strength and dilatancy of granular soil. The dilatancy, for example, was usually explained by a purely sliding model proposed by Newland & Allely in 1957. Basing on experimental observations, Oda (1997) suggested that rolling, rather than sliding, is a dominant micro-deformation mechanism in controlling the dilatancy in a shear band. Even in conventional numerical simulation analyses, particles can move actively by rolling. The problem is that the micro-structure developed in such a simulation analysis is different from that observed in natural sands (Oda 1997; Oda & Kazama, 1998). The difference may arise from the fact that rolling takes place, without mobilizing any rolling resistance at contact points, in such conventional analyses (e.g., Oda 1993). Rolling occurs freely if particles are in contact with their neighboring ones at pure points. Real particles, however, have rough surface texture, and are sometimes covered with a thin film of weathered products. If so, these particles may be in contact with their neighboring ones through contact surfaces, not pure points, so that rolling resistance can play a role to some extent in the contact behavior. Bardet and Huang (1993) showed analytically, as well as experimentally, that the rolling resistance exists even at contacts among cylindrical particles. If so, the huge voids observed by Oda & Kazama (1998) in shear bands can be easily explained: the rolling resistance causes arching action at contact points so that such large voids can be generated during shear deformation.

The objectives of this paper therefore are:

i) to propose a modified version of DEM (called MDEM) by taking into account the rolling resistance at contact points,

ii) to show that MDEM provides a powerful tool for simulating the micro-structure development as well as the overall stress strain relation, and finally

iii) to provide evidence for indicating the real existence of couple stress in numerical simulations.

2. Modified Distinct Element Method (MDEM)

The distinct element method by Cundall (1971) is modified slightly by using an additional element, so that rolling resistance can be activated when rolling takes place at contact points. Only the modified portions are briefly described below since the details have already been given elsewhere (Iwashita and Oda 1998).

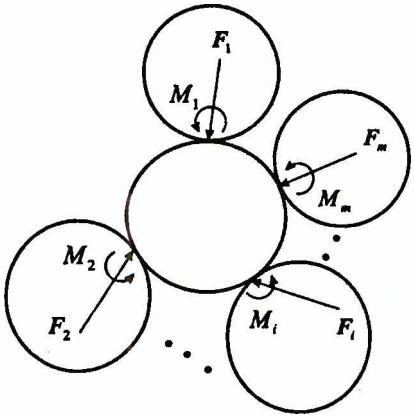

Figure 1. *Contact forces and moments at contact points*

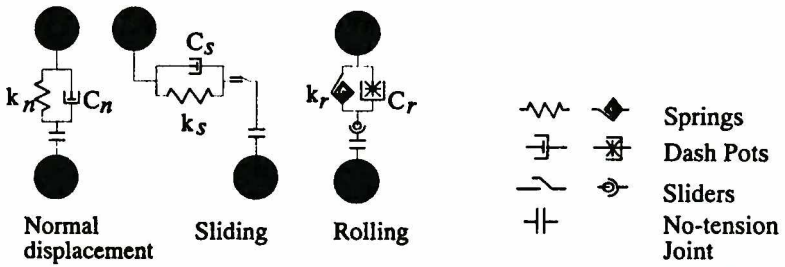

Figure 2. *Contact model in MDEM*

In the conventional DEM, each contact is replaced by a set of normal and shear springs, normal and shear dashpots, normal and shear no-tension joints and a shear slider, and a contact force $\boldsymbol{f}$ is produced as a result of relative movement between two particles in contact (Fig. 1). The contact force, which is resolved into normal N and tangential T forces, is in equilibrium with resistance supplied by the springs and dashpots (Fig. 2). The shear slider starts working at the contact point immediately when N and T satisfy the following inequality:

$$|T| \geq \mu N + c \tag{1}$$

where μ is the coefficient of friction and c is the cohesion (Fig. 3(a)).

Relative movement at a contact point during deformation can be decomposed into two components in general: sliding and rolling (The sliding is related to the tangential force T through a contact law). The rolling leads to relative rotation between two particles at a common contact point (Iwashita and Oda 1998). In order

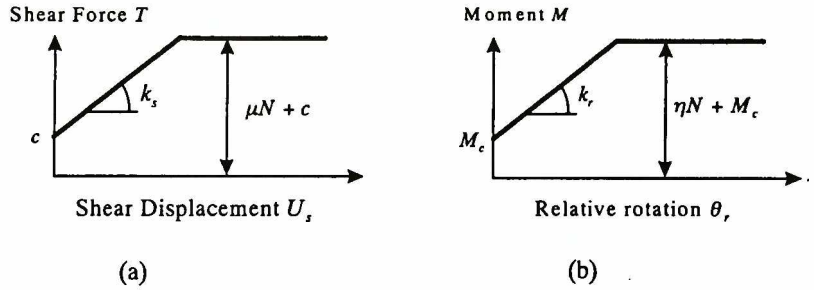

Figure 3. Constitutive model for sliding and rolling at a contact

to relate the relative rotation to contact moment M, an additional set consisting of an elastic spring, a dashpot, a no-tension joint and a slider is installed at each contact point (Fig. 2). The elastic spring yields the rotational resistance equal to $k_r\,\omega$. Here, k_r is the rotational stiffness, and ω denotes the relative rotation by rolling (Iwashita and Oda 1998). The dashpot supplies the rotational resistance equal to $\eta_r d\omega/dt$ where $d\omega/dt$ is the speed of relative particle rotation and η_r is the corresponding viscosity (Fig. 2). The sum of these resistance sources must be in equilibrium with the moment M. The slider starts working, in a similar manner to the shear slider, if the moment satisfies the following inequality (Fig. 3 (b)):

$$|M| \geq \eta N + M_c = \alpha B N + M_c \tag{2}$$

Since η has a similar meaning to the interparticle friction in Eq. (1), it was called the coefficient of rolling friction by Sakaguchi et al. (1993). M_c is the moment arising from a cohesive term. Note that η has a dimension of length. So, it was decomposed into a typical length scale (B; see Fig. 4) and a non-dimensional parameter in Eq. (2). The non-dimensional parameter α controls how much rolling resistance can be generated at contact points. Except that moment is transmitted through contact points, all other aspects of MDEM are exactly the same as those of the conventional DEM.

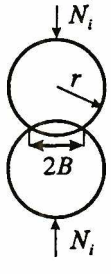

Figure 4. A typical lengh scale B in MDEM

3. Simulation by MDEM

Preparation of Particle Assembly

Disc-like 15840 particles, consisting of three different radii 4 mm, 5 mm and 6 mm, were generated randomly in a loading flame 85 cm × 185 cm.

Mechanical behavior of the assembly depends totally on physical constants

dealing with contact properties, such as normal, shear and rolling stiffness values. Choice of these constants is of great importance, in particular, when simulation results are compared with results obtained from real laboratory tests. In spite of this fact, most of these constants were tentatively chosen on a purely empirical basis, summarized in Table 1. We can do this since our present objective is to show qualitatively that the introduction of the rolling resistance in the conventional DEM has some important effects on the micro-process of shear band development.

Table 1. *Parameters of the simulation and material properties of the sample*

DEM parameters and material properties	**Selcted value**
Number of particles	15840
Radii of the particles	4, 5, 6 mm
Increment of time step (Δt)	1.00×10^{-5} sec
Particle density	2600 kg/m^3
Confining pressure	1.32×10^5 Pa
Inter-particle friction coefficient	0.49
Inter-wall friction coefficient	0.36
Inter-particle cohesion (c)	0.0 N
Normal spring constant (k_n)	1.00×10^8 N/m
Tangential spring constant (k_s)	1.00×10^7 N/m
Damping constant at the contact	0.05
Rolling spring constant (k_r)	7.00×10^2 Nm/rad
Coefficient of rolling damping	1.00×10^{-2} Nm sec/rad
Rolling cohesive moment (M_c)	0.0 Nm

Deformation of the particle assembly was controlled through four boundaries: top, bottom, left and right boundaries. The top and bottom boundaries moved vertically, as loading platens, under either a stress-controlled or a strain-controlled condition. To generate a shear band at a central portion of the assembly, friction was applied between the particles and the top and bottom boundaries (friction coefficient = 0.36).

The left and right boundaries, which are composed of particles (8 mm in radius) linked in chain (Iwashita, et al., 1995). are flexible and can even stretch or shrink like a membrane. No friction worked between the inside particles and the linked particles. End particles in the linked particles were restricted so as to move together with the top and bottom boundaries in the vertical direction. However, they could move freely in the horizontal direction.

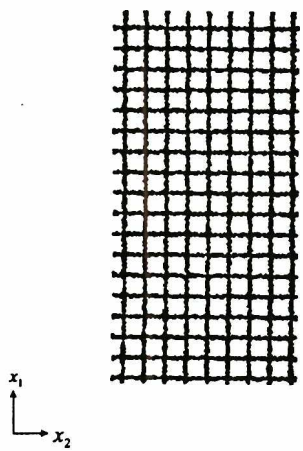

Figure 5. Reference assembly

The assembly was consolidated by applying a uniform stress p_0 on the four boundaries until stress oscillation went down to a negligible level. No gravitational forces were applied during the consolidation. So, the final particle arrangement was considered to be almost isotropic. The consolidated packing is referred to as „reference assembly" in later sections. Particles, which were occasionally aligned in vertical and horizontal directions in the reference assembly, were colored black to trace their movements (Fig. 5). For convenience, orthogonal reference axes x_i $(i = 1,2)$ were chosen as: x_1 is in the vertical direction, and x_2 is in the lateral direction.

Biaxial Compression Tests and Some Results

To run a biaxial test, the vertical stress $\bar{\sigma}_{11}$ was increased, with keeping the lateral stress $\bar{\sigma}_{22}(= p_0)$ kept constant, by moving vertically the top and bottom boundaries step by step. At each movement, calculations were continued in cycle until stress oscillation went down to a negligible level. In doing this, 3×10^5 cycles were needed to complete the whole steps up to the axial strain $\bar{\sigma}_{11} = 5.5\%$, here, the global stresses $\bar{\sigma}_{11}$ and $\bar{\sigma}_{22}$ were calculated using a conventional formula, relating contact forces to stress tensor (e.g., Bardet & Proubet, 1991). The global axial strain $\bar{\varepsilon}_v$ was calculated by dividing the relative displacements between the top and bottom boundaries by the initial height of the reference assembly. The global volumetric strain $\bar{\varepsilon}_v$ in Fig. 6 was also calculated by dividing successive volume changes by the initial volume at the reference assembly.)

Using the same reference assembly, three simulation tests were carried out to examine the effect of the rolling resistance on micro-structure developed in a shear band. In addition to the three tests, many trial tests were done by changing the combination of physical parameters such as k_s, k_n, α and so on. We found that any

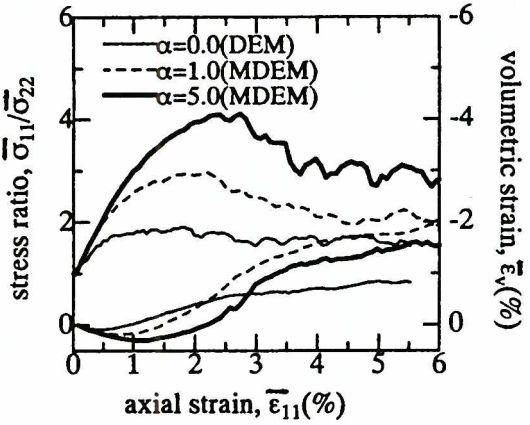

Figure 6. *Stress-strain relationships*

conclusions reported here can be applied to them, in general, irrespective of the choice of these parameters. In each test, the α value was set to 0, 1 or 5. Note that the test using $\alpha = 0$ is equivalent to the conventional DEM, in which no rolling resistance exists at any contact points (called the free rolling test). The two tests using $\alpha = 1$ and =5 are called the rolling resistance tests.

Fig. 6 shows the relationships between the stress ratio $\bar{\sigma}_{11}/\bar{\sigma}_{22}$, the axial strain $\bar{\varepsilon}_{11}$ and the volumetric strain $\bar{\varepsilon}_v$ obtained from the three tests. These curves are similar in shape, i.e., the stress ratio increases up to the corresponding peak, and the volumetric strain is first compressive and is followed by dilatancy. It should be noted, however, that the assembly becomes stronger with increasing α from 0 to 5. It can be said that the rolling resistance at contact points has surely an important effect on the stress ratio mobilized at failure. Furthermore, the following are worth noting: The stress ratio drops only slightly, after the peak, in the free rolling test ($\alpha = 0$). In the rolling resistance tests, on the other hand, the stress ratio drops sharply after the peak. This difference is important since strain softening is commonly associated with strain localization in a dense assembly of granular soils.

4. Results of Numerical Simulation Tests and Their Interpretation

Strain Localization

Particles aligned in vertical and horizontal directions in the reference assembly were colored black to trace their movements. Fig. 7 shows their final positions at $\bar{\varepsilon}_{11}$ = 5.5 %, i.e., (a) is for the case of $\alpha = 0$, (b) is for the case using $\alpha = 1$, and (c) is for the case using $\alpha = 5$. These assemblies were uniformly sheared up to their peak stress ratios at least. As shown in Fig. 7, strain localized to a few shear bands called the shear band, and strain outside the bands was so small that the initial

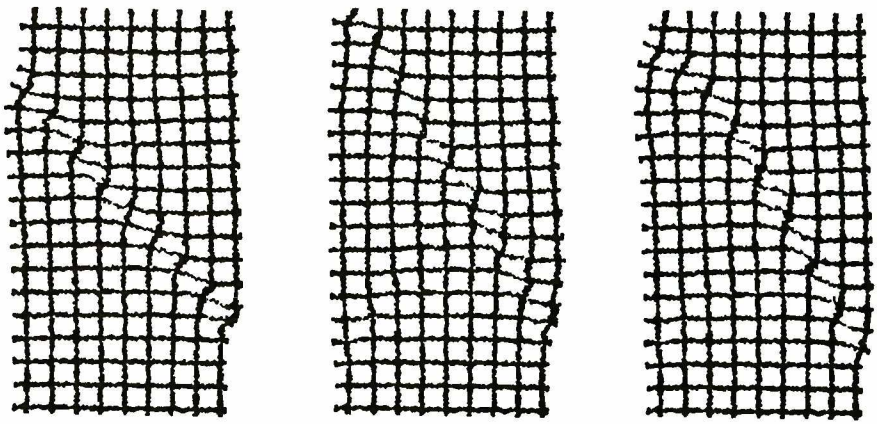

(a) α =0.0 (b) α =1.0 (c) α =0.0

Figure 7. *Strain localization*

configuration of particles almost remained unchanged. Note that similar strain localization takes place irrespective of the choice of α. Iwashita & Oda (1998) showed that no clear shear band was developed in the free rolling test, even after the axial strain was increased by over 10 %. This is because in the case of Iwashita & Oda (1998), numerical tests were carried out using top and bottom platens with friction less boundaries. Shear bands are clearly developed in the present tests in which the top and bottom are composed of frictional boundaries (μ = 0.36).

Column-Like Structure

Oda et al. (1982) observed the column-like structure (called the column) extending parallel to a major principal stress direction in photoelastic pictures taken from biaxial tests on two-dimensional assemblies of rod-like particles. The major (axial) stress was mainly transmitted through the columns. Results of the present simulation tests also showed that highly stressed particles are aligned, like column, parallel to the vertical direction in each of the tests. It can be said accordingly that the column-like structure is a common feature developed during a strain hardening process not only in real assemblies (e.g., Wakabayashi, 1957; Drescher, 1976; Oda1972; and Oda et al.,1982) but also in simulation model assemblies (Iwashita & Oda 1998).

Particle Rotation

It is well known that particle rotation plays a dominant role in developing shear bands in granular assemblies (Bardet & Proubet, 1991 & 1992; Oda 1997; and Oda & Kazama, 1997). Particles rotation during the deformation from $\bar{\varepsilon}_{11}$ = 0 % to 5.5 % is shown in Fig. 8, where the black circles denote counterclockwise rotation by more than 10º (positive), while the white ones denote clockwise rotation by more than 10º (negative). Note that particle rotation occurs extensively in some limited zones.

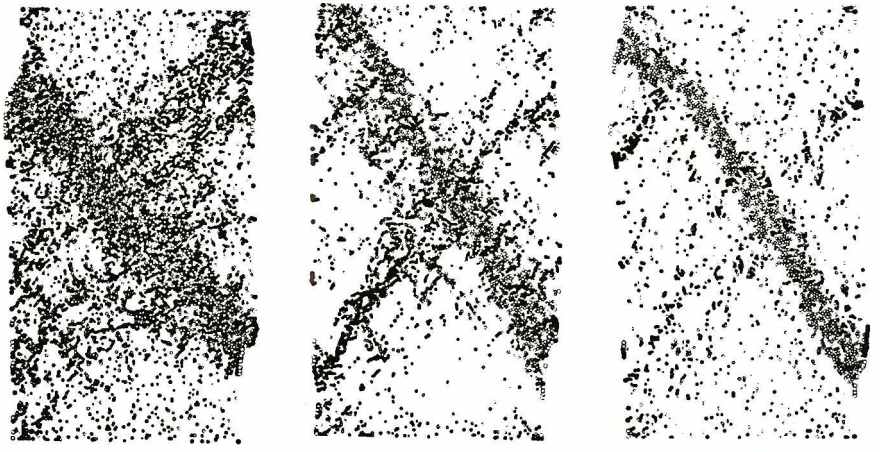

(a) α =0 (b) α =1 (c) α =5

Figure 8. *Particle rotation*

Especially in the rolling resistance tests using $\alpha = 1$ and 5 (Figs 8 (b) and (c)), the highly rotated particles only appear in the distinct zones where the shear strain was highly accumulated (Figs 7(b) and (c)).

Particle rotation commonly occurs, irrespective of the α values, during a shear banding process. It should be noted, however, that there is a marked difference between them. In the free rolling test using $\alpha = 0$ (Fig. 8 (a)), particles which rotate by more than 10^{o} are dispersed so widely that shear bands are not clearly defined. More importantly, the rotation takes place either clockwise or counterclockwise at the same rate. In the rolling resistance tests using $\alpha = 1$ and 5 (Fig. 8 (b) and (c)), on the other hand, such highly rotated particles are concentrated inside the shear bands. Clockwise rotation mainly occurs in shear bands running from upper left to lower right, while counterclockwise rotation occurs in the corresponding conjugate shear bands.

Fig. 9 is prepared to see more precisely where particle rotation takes place: (a) is for the free rolling test, and (b) is for the rolling resistance test using $\alpha = 5$. In these figures, cumulative rotation (in radians) taking place between the specified axial strain increments is plotted against the distance of the particle from a center line of a shear band (normalized by the mean particle diameter). Two points can be noted: particles extensively rotate inside the shear band in both the free rolling and rolling resistance tests. In the rolling resistance test, however, the rotation direction is skewed in the negative side so that a high particle rotation gradient is developed. This result means that the particle rotation gradient is generated only when rolling resistance is implemented at contact points.

The difference in particle rotation can be explained as follows: When rolling occurs between two neighboring particles, clockwise rotation of a particle causes counterclockwise rotation of the counter particle, so the clockwise and

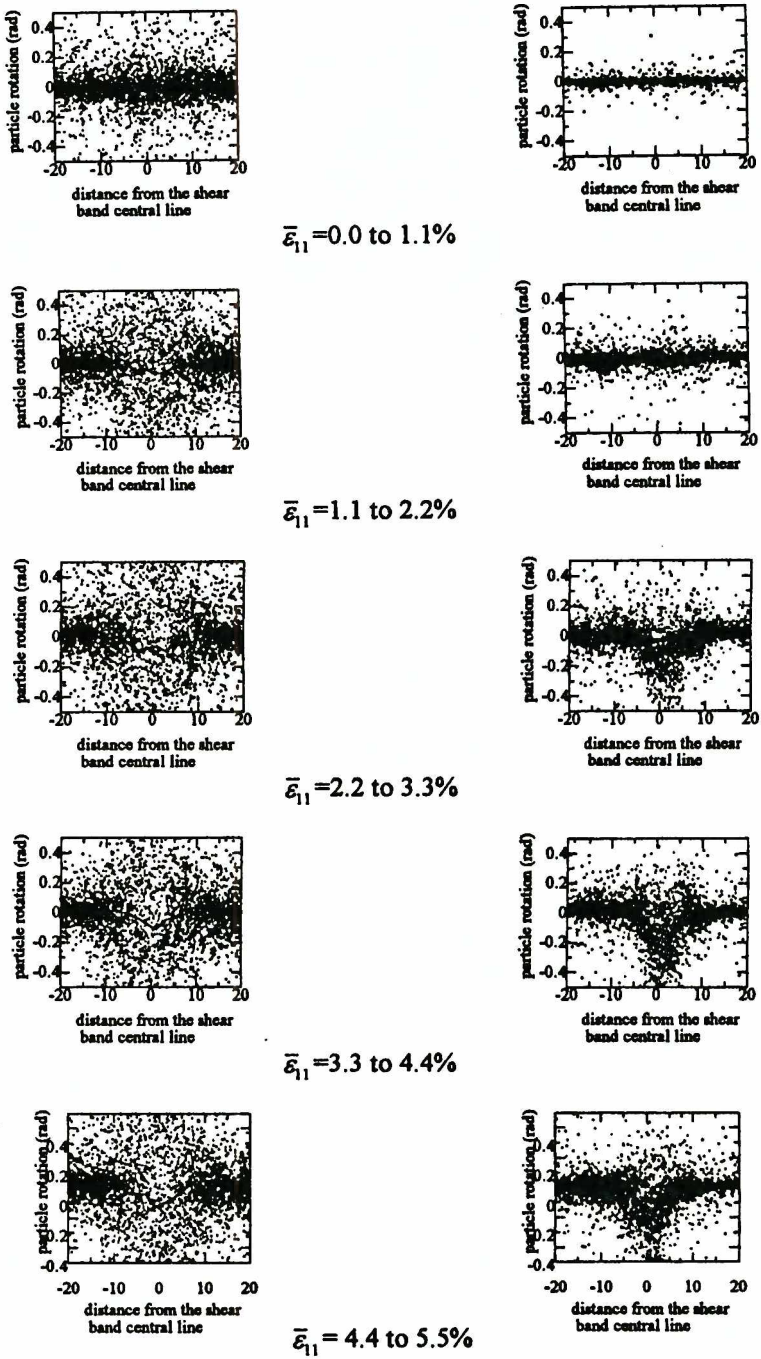

Figure 9. Distributiom of particle rotation

(a) Association of clockwise and counterclockwise rotation

(b) Particle rotations in column-like structure

Figure 10. *Two types of particle rotation by rolling*

counterclockwise rotations tend to appear equally during deformation (Fig. 10 (a)). This really happens in the free rolling test. What happens if particles involved in a column are rotated by rolling? In this case, upper particles roll over lower ones (Fig. 10 (b)). As a result, the column is bent clockwise as a whole, and clockwise rotation of particles may be more likely to occur than counterclockwise rotation. In the rolling resistance test, as discussed in the previous section, column-like structure was developed during a strain hardening process, up to the peak stress ratio, parallel to the vertical. After the peak, the structure was bent clockwise, in a manner similar to Fig. 10 (b). It can be concluded therefore that bending of column-like structure causes clockwise rotation of particles in a shear band such that a high particle rotation gradient is generated.

Localization of Volumetric Strain

The most important observation in the rolling resistance test was that large voids are aligned in shear bands (see Iwashita and Oda (1998)). This means that volumetric strain (dilatation) is concentrated, especially after failure, into these narrow bands, and that the strain softening behavior in Fig. 6 certainly results from the weakening of the shear bands.

Lagrange's strain tensor was calculated to examine more precisely progressive accumulation of volumetric strain in a specimen. To do this, a small circle with its center at a center of each circular particle was inscribed in particle configuration at $\bar{\varepsilon}_{11} = \bar{\varepsilon}_{11}^{(1)}$, such that a sufficient number (about 10) of particles was involved in it. All particle centers in the small circle were displaced while the global strain was increased from $\bar{\varepsilon}_{11}^{(1)}$ to $\bar{\varepsilon}_{11}^{(2)}$. Using these displacement data, Lagrange's (local) strain increment tensor and the corresponding volumetric strain increment $\Delta\varepsilon_v$ were calculated by means of the least square method. Fig. 11 shows the spatial distributions of $\Delta\varepsilon_v$ at five successive stages in the rolling resistance test using $\alpha = 5$. The white circles denote the compressive volumetric strain by more than 3 %, while the black ones denote expansive volumetric strain by more than 3 %. The following results are worth noting:

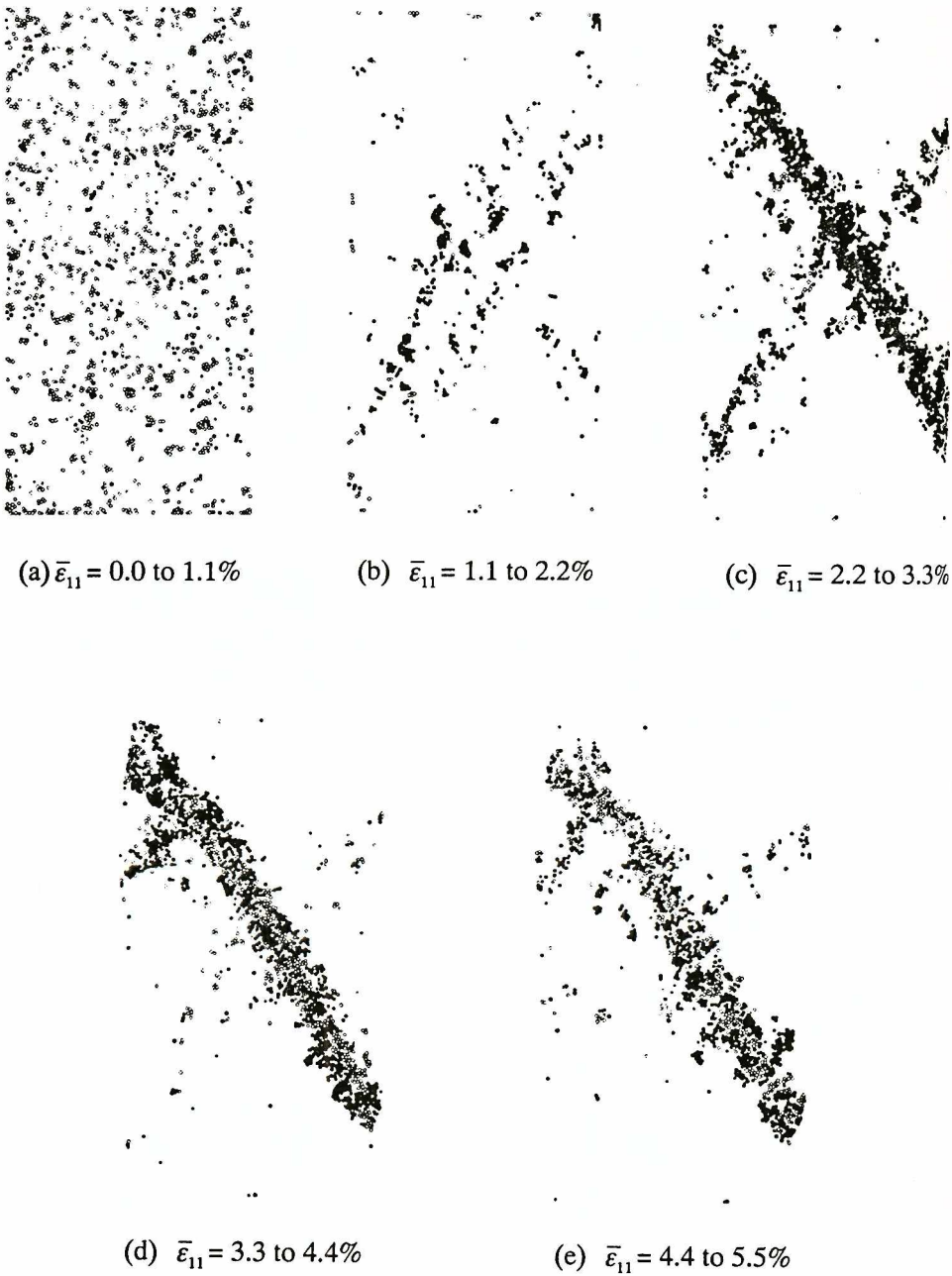

Figure 11. *Distribution of incremental volumetric strain: $\alpha = 5.0$*

1) Note, in Fig. 6, that the global volumetric strain $\bar{\varepsilon}_v$ in the rolling resistance test is compressive during the global deformation from $\bar{\varepsilon}_{11} = 0$ to 1.1 %. As seen in Fig. 11 (a), the local volumetric strain increment is also mostly compressive. More importantly, it is distributed uniformly all over the specimen without any localization to some zones. This is a typical process taking place during the so-called strain hardening.

2) When the global strain $\bar{\varepsilon}_{11}$ reaches 2.2 %, the specimen fails, and the global volumetric strain turns out to be dilatative (Fig. 6). Fig. 11 (b) shows that locations where dilatation takes place are localized in several potential shear bands. It is interesting to note that a shear band, which mainly dilates in the next stage (Fig. 11(c)), does not dilate at this stage at all.

3) When the global strain $\bar{\varepsilon}_{11}$ reaches 2.2 to 3.3 %, strain softening starts in parallel with extensive dilatancy. At this stage, as shown in Fig. 11 (c), the dilatational volumetric strain is gradually concentrated into the main shear band shown in Fig. 7 (c).

4) The assembly reaches a residual state at $\bar{\varepsilon}_{11} = 3.3$ % to 5.5 %. The local strain continues to be concentrated to the main shear band. At this stage, both compression and dilatancy occur simultaneously in the shear band (Fig. 11 (d) and (e)), so that the volumetric strain, if averaged over the shear band, becomes constant. It is very interesting to know that large voids are generated and collapsed simultaneously in a shear band during a residual state: that is, the generation is balanced with the collapse.

Couple Stress Developed in Shear Band

To study a stress state developed in a shear band, the rolling resistance test using $\alpha = 5.0$ was analyzed in some detail. To obtain this, the specimen sheared up

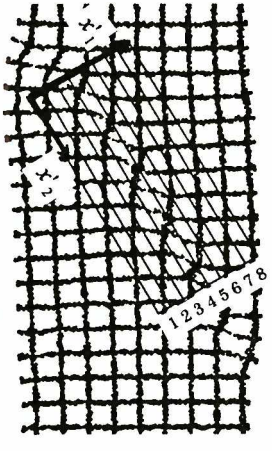

Figure 12. Observation bands

to $\bar{\varepsilon}_{11} = 5.5$ % was divided into eight square bands, named 1 to 8 in Fig. 12, parallel to shear band boundaries. Based on all data shown in Figs 7 to 11, it can be considered that bands 4 to 5 are located inside the main shear band seen in Fig 7, and that the boundary between bands 4 and 5 is very close to a central line in the shear band. All the boundaries between these bands were traced back until $\bar{\varepsilon}_{11} = 0$ % such that all particles remained in the same band during deformation.

Local stress $\hat{\sigma}_{ij}$ and local couple stress $\hat{m}_{ij}$ were calculated using contact forces f_i^a and contact moments m_i^a acting on all contact points belonging to each band, as follows (Oda & Iwashita, 1998);

$$\hat{\sigma}_{ji}^{(k)} = \frac{1}{V^{(k)}} \sum_{a=1}^{N^{(k)}} l^a f_i^a n_j^a \tag{3}$$

$$\hat{m}_{ji}^{(k)} = \frac{1}{V^{(k)}} \sum_{a=1}^{N^{(k)}} l^a m_i^a n_j^a \tag{4}$$

where l^a is the branch length of the a-th contact, $N^{(k)}$ is the total number of contact points in a k-band and $V^{(k)}$ is the volume of the band. For convenience, local axes x_1' and x_2' were selected in the directions perpendicular and parallel to the shear band boundaries, respectively, and any stress components were calculated with respect to the local axes. Note that $\hat{m}_{ji}$ has non-zero component when i is set to 3 in two-dimensions, i.e., $\hat{m}_{1'3'}$ and $\hat{m}_{2'3'}$ are non-zero couple stress components acting on the two planes parallel and perpendicular to the shear band boundary, respectively.

Fig. 13 shows the successive change of couple stress $\hat{m}_{1'3'}$ during deformation in which the abscissa is the band number 1 to 8. No couple stress is developed in the band before a peak stress state ($\bar{\varepsilon}_{11} < 2.2$ %; also see Fig. 6). When the specimen is deformed beyond the peak, however, the couple stress becomes large in bands 4 and 5. The couple stress remains small in bands 3 and 10 which are located outside the shear band. More importantly, the sign of $\hat{m}_{1'3'}$ changes from negative to positive, in a consistent manner with the change of the particle rotation gradient reported in Fig 9 (b). A similar result was reported in the result of the micropolar-continuum theory by Tejchman (1998). We also observed the non-symmetry of stress tensor, i.e. $\hat{\sigma}_{12} \neq \hat{\sigma}_{21}$. However, the difference is very small as discussed by Oda (1998). A similar, but very small, change of $\hat{m}_{1'3'}$ was also observed in the case of the test using $a = 1$. Of course, no couple stress is developed in the free rolling test using $a = 0$.

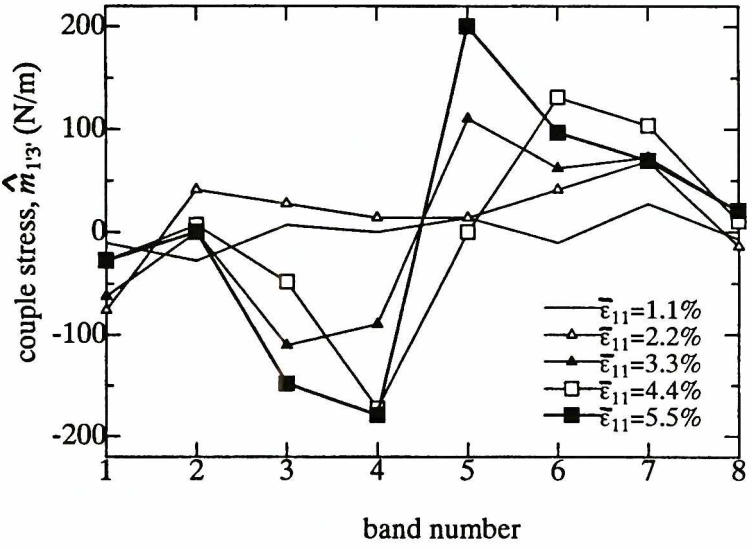

Figure 13. *Change of couple stress m*

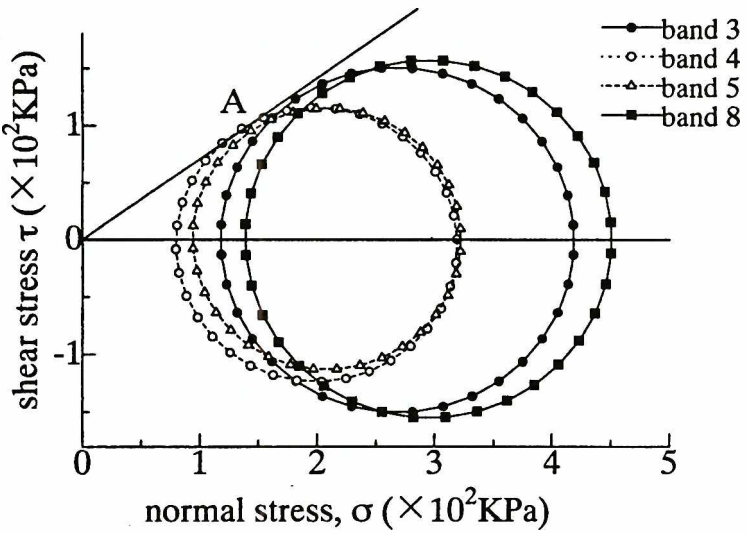

Figure 14. *Mohr's stress circle*

Fig. 14 shows Mohr's stress circles: the solid circles are for bands 3 and 8 which are located outside the shear band, and the dotted circles for bands 4 and 5 which are located inside the shear band. In bands 3 and 8, the major and minor stresses almost coincide with the stresses applied to the boundaries of the assembly, and their principal directions are almost parallel to the vertical and horizontal directions, respectively. The stresses acting in the shear band yield much smaller stress circles. The major principal stress axes in bands 3 and 4 are both inclined to the vertical direction at about 20°. Furthermore, the following three points are worth

noting: i) the solid and dotted stress circles are both tangent to a common failure line; ii) the normal and shear stresses acting on a plane parallel to the shear band boundaries are given by a point A in Fig. 14 where the solid and dotted stress circles are intersected; and iii) the centers of stress circles are almost on the abscissa. This second observation strongly suggests that the stress jumps discontinuously along a boundary between the outside and inside of the shear band (e.g., see Vermeer, 1990). The third one says that the stress tensor is almost symmetrical in spite of the existence of couple stress. In other words, the magnitude of couple stress is much smaller than that of stress. In fact, the normalized couple stress, $\hat{m}_{1,3,}/(\hat{\sigma}_{kk}d_{50})$, is about 0.04 ($d_{50}$ is the mean diameter).

5. Conclusion

Numerical tests were carried out to simulate micro-structure of shear bands developed in dense sands, as well as their overall stress-strain behavior. To do this, conventional distinct element method (DEM) was modified in such a way that the effect of rolling resistance at contact points was taken into account (MDEM). Three new findings, which seem of particular importance in the study of the shear banding process of granular media, are summarized below:

1) The development of shear bands can well be simulated when the rolling resistance is considered in the conventional DEM. That is, not only the generation of large voids inside a shear band but also the high gradient of particle rotation along the shear band boundaries can both be reproduced, in a quite similar manner to those of the natural granular soils.

2) In the simulation tests using MDEM, couple stress is generated, at an appreciable amount, and changes its sign from negative to positive. This observation is consistent not only with the change in the particle rotation gradient reported here, but also with the result from the micropolar-continuum theory. The stress tensor is non-symmetric, i.e., $\hat{\sigma}_{12} \neq \hat{\sigma}_{21}$. However, the difference is very small.

3) We can also point out the possibility that the stress can discontinuously jump when crossing shear band boundaries.

Acknowledgement

We express our sincere thanks to Mr. T. Kakiuchi and I. Hashimoto who helped us a lot with doing the numerical simulation tests as a part of the master and graduation thesis at Saitama University.

References

[1] Bardet J. P., (1994), *Observations on the effects of particle rotations on the failure of idealized granular materiall*, Mechanics of Materials, Elsevier, Amsterdam, Netherlands, Vol.18, 159-182

[2] Bardet J. P., Proubet J., (1991), *A numerical investigation of the structure of persistent shear bands in granular media*, Geotechnique, London, UK, Vol.41, No.4, 599-613

[3] Bardet J. P., Proubet J., (1992), *Shear-band analysis in idealized granular material*, Journal of Engineering Mechanics, ASCE, Vol.118, No.2, 397-415

[4] Bardet J. P., Huang Q., (1993), *Rotational stiffness of cylindrical particle contacts*, Proc. Second Int. Conf. on Micromechanics of Granular Media, Birmingham, (ed. C. Thornton), Balkema, Rotterdam, Netherlands, 39-43

[5] Bathurst R. J., Rothenburg L., (1990), *Observations on stress-force-fabric relationships in idealized granular materials*, Mechanics of Materials, Elsevier, Amsterdam, Netherlands, Vol.9, 65-80

[6] Cundall P. A., (1971), *A computer model for simulating progressive, large scale movement in blocky rock system*, Proc. Symp. Int. Soc. Rock Mech., Nancy, France, Vol.2, No.8

[7] Cundall P. A., Strack, O. D. L., (1979), *A discrete numerical model for granular assemblies*, Geotechnique, London, UK, Vol.29, No.1, 47-65.

[8] Desrues J., Chambon R., Mokni, M., Mazerolle, F., (1996), *Void ratio evolution inside shear bands in triaxial sand specimens studied by computed tomography*, Geotechnique, London, UK, Vol.46, No.3, 529-546

[9] Drescher A., (1976), *An experimental investigation of flow rule for granular materials*, Geotechnique, London, UK, Vol.26, No.4, 591-601

[10] Finno R. J., Harris W. W., Mooney, M. A., Viggiani, G., (1996), *Strain localization and undrained steady state of sand*, Journal of Geotechnical Engineering, ASCE, Vol. 122, No. 6, 462-473

[11] Horne M. R., (1965), *The behavior of an assembly of rotund, rigid, cohesionless particles I and II*, Proc. Royal Soc., London, UK, Vol. A 286, 62-97

[12] Iwashita K., Matsuura K., Oda M., (1995), *Distinct element method with the effect of moment transfer at the contact points*, Journal Geotechnical Engineering, Tokyo, Japan, No.529/III-33, 145-154 (in Japanese)

[13] Iwashita K., Oda M., (1998), *Rolling resistance at contacts in the simulation of shear band development by DEM*, Journal of Engineering Mechanics, ASCE, No.124, 285-292

[14] Ke T. C., Bray J. D., (1995), *Modeling of particulate media using discontinuous deformation analysis*, Journal of Engineering Mechanics, ASCE, No.121, 1234-1243

[15] Matsuoka H., (1974), *Stress-strain relationship of sands based on the mobilized plane*, Soils & Foundations, Tokyo, Japan, Vol.14, No.2, 47-61

[16] Mühlhaus H. B.,Vardoulakis, I., (1987), *The thickness of shear bands in granular materials*, Geotechnique, London, UK, Vol.37, No.3, 271-283

[17] Nemat-Nasser S., (1980), *On behavior of granular materials in simple shear*, Soils & Foundations, Tokyo, Japan, Vol.20, No.3, 59-73

[18] Newland P. L., Allely, B. H., (1957), *Volume changes in drained triaxial tests on granular materials*, Geotechnique, London, UK, Vol.7, 17-34

[19] Oda M., (1972), *Deformation mechanism of sand in triaxial compression tests*, Soils and Foundations, Tokyo, Japan, Vol.12, No.4, 45-63

[20] Oda M., (1993), *Micro-fabric and couple stress in shear bands of granular materials*, Proc. Second Int. Conf. on Micromechanics of Granular Media, Birmingham, (ed. C. Thornton), Balkema, Rotterdam, Netherlands, 161-166

[21] Oda M., (1997), *A micro-deformation model for dilatancy of granular materials*, Symposium on Mechanics of Particulate Materials in McNu Conference, (ed. C. S. Chang), ASCE, 24-37

[22] Oda M., (1998), *Particle rotation and couple stress*, In Introduction to Mechanics of Granular Materials, (eds: M. Oda and K. Iwashita), Balkema (to be published)

[23] Oda M, Iwashita K., (1998), *Couple stress developed in shear bands* (1); Particle rotation and couple stress in granular media (in print)

[24] Oda M., Kazama H., (1998), *Micro-structure of shear band and its relation to the mechanism of dilatancy and failure of granular soils*, Geotechnique, London, UK (to appear)

[25] Oda M., Konishi J., Nemat-Nasser S., (1982), *Experimental micro-mechanical evaluation of strength of granular materials: Effect of particle rolling*, Mechanics of Materials, Elsevier, Amsterdam, Netherlands, Vol.1, 267-283

[26] Rowe P. W., (1962), *The stress-dilatancy relation for static equilibrium of an assembly of particles in contact*, Proc. Royal Soc., London, UK, Vol. A 269, 500-527

[27] Sakaguchi H., Ozaki E., Igarashi T., (1993), *Plugging of the flow of granular materials during the discharge from a silo*, International Journal of Modern Physics Vol. B 7, 1949-1963

[28] Scarpelli G., Wood D. M., (1982), *Experimental observations of shear band patterns in direct shear tests*, Proc IUTAM Symp. Deformation and Failure of Granular Material, Delft, (eds. P. A. Vermeer, H. J. Luger), Balkema, Rotterdam, Netherlands, 473-484

[29] Tatsuoka F., Nakamura S., Huang C. C., Tani K., (1990), *Strength anisotropy and shear band direction in plane strain tests of sand*, Soils & Foundations, Tokyo, Japan,Vol.30 No. 1, 35-54

[30] Tejchman J., (1998), *Numerical modelling of shear localisation with a polar hypoplastic model*, Localisation and Bifurcation Theory for Soils and Rocks, ed. by F. Oka, 1998 (in print)

[31] Thomas A. P., Bray J. D., Ke T. C., (1996), *Discontinuous deformation analysis for soil mechanics*, First International Forum on Discontinuous Deformation Analysis, Berkeley, USA

[32] Vermeer P. A., (1990), *The orientation of shear bands in biaxial tests*, Geotechnique, London, UK, Vol.40, No.2, 223-236

[33] Wakabayashi T., (1957), *Photoelastic method for determination of stress in powdered mass*, Proc. Seventh Japan Nat. Congr. Appl. Mech., Tokyo, Japan, 153-158

[34] Yoshida T., Tatsuoka F., Siddiquee M.S.A. Kamegai, Y., Park C.-S., (1994), *Shear banding in sands observed in plane strain compression*, Symp. Localization and Bifurcation Theory for Soils and Rocks, (eds. R. Cambou, J. Desrues and I. Vardoulakis), Balkema, Rotterdam, Netherlands, 165-179